Oxygen tongues and zonal currents in the equatorial Atlantic

Peter Brandt, Verena Hormann, Bernard Bourlès, Jurgen Fisher, Friedrich Schott, Lothar Stramma, Marcus Dengler

Oxygen tongues and zonal currents in the equatorial Atlantic

Peter Brandt,[1] Verena Hormann,[1] Bernard Bourlès,[2] Jürgen Fischer,[1]
Friedrich A. Schott,[1] Lothar Stramma,[1] and Marcus Dengler[1]

Received 4 July 2007; revised 3 December 2007; accepted 8 January 2008; published 12 April 2008.

[1] Equatorial zonal currents and associated oxygen distributions are studied using shipboard hydrographic data, trajectories from isopycnic floats drifting at about 300 m depth, and velocity time series from the upper 1100 m obtained at two equatorial moorings located at 35°W and 23°W. Mean profiles of zonal velocity measured by moored acoustic Doppler current profilers yielded a westward flowing Equatorial Intermediate Current (EIC) below the Equatorial Undercurrent (EUC) at both locations. The EIC consists of two westward current cores at about 250 and 450 m. The upper core of the EIC deepens by about 30 m from 23°W, where it has a mean velocity of 6 ± 2 cm s^{-1}, to 35°W, where the mean is 5 ± 3 cm s^{-1}. The lower core of the EIC is about twice as strong with 12 ± 1 cm s^{-1} at 23°W and 9 ± 2 cm s^{-1} at 35°W. The flow below the EUC is characterized by substantial interannual variability. From May to December 2005 a strong, zonally coherent eastward jet occurred at 300 to 350 m depth, found to be an expression of shallow stacked jets superimposed on the mean EIC. Shipboard hydrographic observations in June–July 2006 revealed the existence of a high-oxygen tongue that can be traced from 35°W to 10°W in the depth range of the eastward jet prevailing during the preceding year. On the basis of an advection-diffusion balance, it is suggested that the oxygen decrease from 35°W to 10°W within the oxygen tongue is mainly balanced by lateral eddy diffusivity and oxygen consumption, with diapycnal turbulent diffusivity playing only a minor role.

Citation: Brandt, P., V. Hormann, B. Bourlès, J. Fischer, F. A. Schott, L. Stramma, and M. Dengler (2008), Oxygen tongues and zonal currents in the equatorial Atlantic, *J. Geophys. Res.*, *113*, C04012, doi:10.1029/2007JC004435.

1. Introduction

[2] The equatorial Atlantic Ocean is characterized by vigorous zonal currents. In the thermocline layer, the eastward flowing Equatorial Undercurrent (EUC) transports 15 to 20 Sv (decreasing from west to east) from the western boundary toward the eastern equatorial Atlantic [*Schott et al.*, 2003; *Brandt et al.*, 2006]. This current is the primary equatorial current branch of the Subtropical Cells (STCs) that connect the subtropical subduction regions of both hemispheres with the equatorial Atlantic upwelling regions [*Liu et al.*, 1994; *McCreary and Lu*, 1994; *Malanotte-Rizzoli et al.*, 2000; *Schott et al.*, 2004]. Additionally, the EUC is one of the main warm water routes of the Meridional Overturning Circulation (MOC) of the Atlantic Ocean. By analyzing model results, *Hazeleger and de Vries* [2003] found that about 2/3 of the EUC transport at 20°W contributes to the MOC of the Atlantic and about 1/3 recirculates within the STC flow. While the mean transport of the EUC is well established in the western and central equatorial Atlantic using direct shipboard current observations, these observations are not conclusive regarding the seasonal and longer-term variability of the EUC transport mainly owing to pronounced intraseasonal variability [*Hormann and Brandt*, 2007].

[3] Below the EUC, a mean westward flow associated with the Equatorial Intermediate Current (EIC) was observed in the shipboard velocity measurements mentioned above. The EIC transport was estimated to be about 10 Sv between $\sigma_\theta = 26.8$ kg m^{-3} (about 300 m) and $\sigma_1 = 32.15$ kg m^{-3} (about 1150 m) at 35°W [*Schott et al.*, 2003]. Out of the 10 Sv at 35°W, about 6 Sv are transported between $\sigma_\theta = 26.8$ kg m^{-3} and 700 m, which is the same value estimated at 26°W [*Brandt et al.*, 2006]. Up to now, the observed westward EIC level flow with mean velocities above 5 cm s^{-1} could not be reproduced by state-of-the-art numerical models, and *Jochum and Malanotte-Rizzoli* [2003] suggested that the shipboard measurements represented snapshots in time that were biased by seasonal Rossby waves. However, recent moored observations at 23°W confirmed the presence of westward mean current cores below the EUC [*Brandt et al.*, 2006]. Here we will build on these earlier results using an extended data set including moored data from the successive deployment period at 23°W as well as from an additional equatorial mooring at 35°W.

[1] IFM-GEOMAR, Leibniz-Institut für Meereswissenschaften, Kiel, Germany.
[2] Centre IRD de Brest, Plouzané, France.

0148-0227/08/2007JC004435

[4] A strong seasonal cycle of the flow in the depth range of the EIC as suggested by different model studies [*Jochum and Malanotte-Rizzoli*, 2003; *Thierry et al.*, 2004] is in general agreement with recent observations of seasonal variability of the equatorial current and density fields [*Brandt and Eden*, 2005]. This variability can be best described by equatorial Kelvin and Rossby beams represented by the first few baroclinic modes [*McCreary*, 1984]. At intermediate depths (as well as at larger depth) the zonal circulation often shows the presence of vertically alternating eastward and westward jets with short vertical length scales [e.g., *Ponte et al.*, 1990; *Gouriou et al.*, 2001]. In the deep water layers of the central equatorial Atlantic, eastward jets are associated with a maximum in Chlorofluorocarbon (CFC) concentration indicating advection of newly formed North Atlantic Deep Water from the western boundary toward the interior Atlantic [*Andrié et al.*, 1998; *Gouriou et al.*, 2001; *Bourlès et al.*, 2003]. These so-called Equatorial Deep Jets (EDJs) or stacked jets are in general not well represented in present general circulation models, probably because their simulation requires very high vertical and horizontal resolutions [*d'Orgeville et al.*, 2007; *Eden and Dengler*, 2008].

[5] At thermocline and intermediate levels, the western boundary regime is characterized by an oxygen maximum, while the eastern part of the basin is occupied by low-oxygen waters. The strong gradient in the oxygen concentration along the equator is the reason why eastward and westward flows in the equatorial Atlantic can often be identified by high and low oxygen values, respectively. While the (eastward decreasing) oxygen maximum in the thermocline layer associated with the EUC is located directly on the equator [*Metcalf and Stalcup*, 1967; *Tsuchiya et al.*, 1992; *Schott et al.*, 1995], high oxygen values at intermediate depths are typically associated with the eastward flowing Southern and Northern Intermediate Countercurrents (SICC and NICC) located at about 2°S and 2°N [*Tsuchiya et al.*, 1992; *Schott et al.*, 1995; *Boebel et al.*, 1999; *Bourlès et al.*, 2002]. Particularly, the NICC had been identified as a supply pathway of high-oxygen waters toward the oxygen minimum zone of the tropical North Atlantic [*Stramma et al.*, 2005].

[6] Here we report on new current and hydrographic observations that allow identification of the mean and interannually varying equatorial circulation and its effects on the oxygen distribution in the equatorial belt. These observations include velocity records obtained with acoustic Doppler current profilers (ADCPs) moored at the equator at 35°W and 23°W, trajectories from isopycnic RAFOS floats drifting at the potential density surface σ_θ = 26.8 kg m^{-3} (about 300 m) and hydrographic and current data from shipboard measurements (section 2). Velocities obtained from the current meter moorings together with the float trajectories allow a coherent description of the equatorial zonal flow field during the period February 2004 to June 2006 (section 3). The equatorial oxygen distribution observed during R/V *Meteor* cruise 68/2 in June–July 2006 is then analyzed in relation to the jet-like structures found in the moored velocity observations (section 4). Previous shipboard oxygen measurements are additionally used to discuss the interannual variability in the observed flow and tracer fields (section 5) and finally, in section 6, the results are summarized and their potential relevance for the ventilation of the off-equatorial oxygen minimum zones is discussed.

2. Observations

2.1. Shipboard Measurements

[7] The analysis of shipboard measurements is mainly based on data obtained during R/V *Meteor* cruise 68/2 in June–July 2006 in the equatorial Atlantic between 2°N and 2°S and between 35°W and 10°W. During this cruise hydrographic and ADCP current data were collected along three meridional sections crossing the equator at 35°W, 23°W, and 10°W (see Figure 1) as well as along two zonal sections running along the equator and 2°N, respectively, between 23°W and 10°W. The meridional section along 23°W from the equator to the Cape Verde Islands cutting through the oxygen minimum zone of the tropical North Atlantic is studied in detail by *Stramma et al.* [2008]. Hydrographic and current data taken during previous cruises along selected meridional sections in the central equatorial Atlantic will be used for comparison. Velocity data from these earlier surveys and other available sections were evaluated by *Brandt et al.* [2006] and *Hormann and Brandt* [2007] with respect to the mean and seasonal cycle of the zonal flow.

[8] The CTD work during R/V *Meteor* cruise 68/2 was carried out with a Seabird Electronic 9plus CTD system with oxygen sensors. The readings of two temperature sensors with independent calibrations differed by less than ±0.001°C and the accuracy was estimated to be of the order of this difference. Salinity and oxygen sensors were calibrated versus water samples and salinity and oxygen accuracies of ±0.002 and ±1.3 μmol kg^{-1}, respectively, were obtained. CTD station spacing was 20′ of latitude from 2°S to 3°N and 30′ of latitude north and south of it along the meridional sections and 1° of longitude along the zonal sections.

[9] Two vessel-mounted RDI Ocean Surveyors working at frequencies of 75 kHz (OS75) and 38 kHz (OS38), respectively, were used for underway current observations. These instruments have phased array transducers and depth ranges of up to 750 m (OS75) and 1200 m (OS38). Navigation information was supplied to the ADCP units from a 3D ASHTECH GPS. During post processing, misalignment angles and amplitude factors were obtained from water track calibration. Uncertainties of 1h averages were 1–3 cm s^{-1}, similar to what has been achieved during previous cruises with the same instrumentation [*Fischer et al.*, 2003].

2.2. Moored Observations

[10] Data from two equatorial current meter moorings located near 35°W and 23°W will be analyzed here. The mooring at 35°W was deployed on 13 August 2004, during R/V *Meteor* cruise 62/2 and recovered on 6 June 2006, during R/V *Meteor* cruise 68/2. The exact mooring position was 0°5.8′N, 35°1.2′W. The mooring contained two 150-kHz narrowband ADCPs looking upward and downward from about 150 m depth at vertical resolutions of about 9 m and 17m, respectively (Table 1). The measurement range of these ADCPs is typically 350 m. At 500 m, 652 m, 809 m,

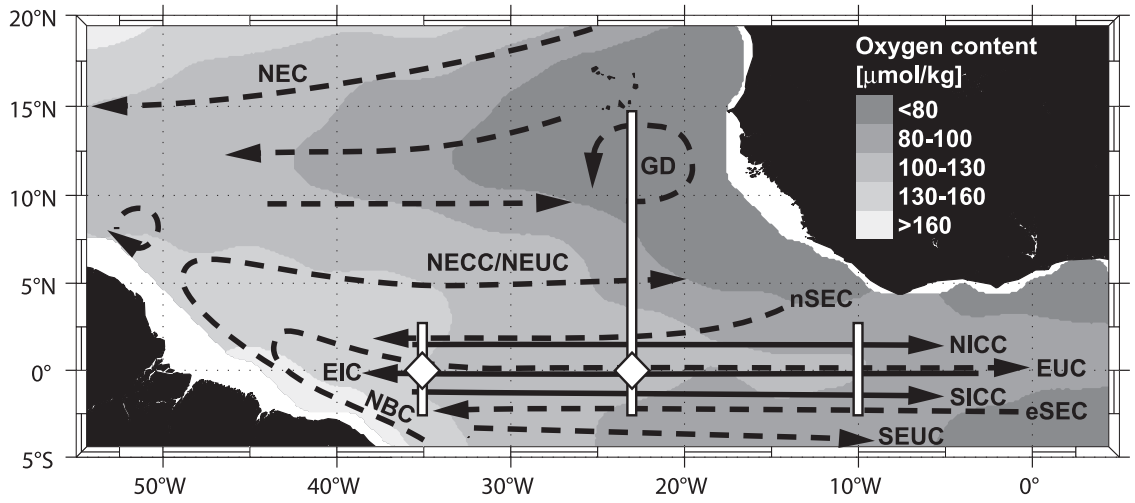

Figure 1. Schematic diagram of the shallow subtropical and tropical Atlantic circulation superimposed on the climatological distribution of oxygen content (μmol kg^{-1}) at 300–500 m depth (based on the climatology of *Gouretski and Jancke* [1998]). Also shown are the locations of the equatorial moorings at 35°W and 23°W (diamonds) and of meridional shipboard current-profiling sections. Surface and thermocline current branches marked (dashed) are North Equatorial Current (NEC), northern and equatorial branches of the South Equatorial Current (nSEC and eSEC), North Equatorial Countercurrent (NECC), North Brazil Current (NBC), North and South Equatorial and Equatorial Undercurrents (NEUC, SEUC, and EUC), and the cyclonic circulation around the Guinea Dome (GD). Intermediate current branches marked (solid) are Northern and Southern Intermediate Countercurrents (NICC and SICC) and Equatorial Intermediate Current (EIC).

and 1107 m Sontek (Argonaut) acoustic current meters were used. The mooring at 23°W was deployed several times, supported by different projects/programs. Here, we will use data from two successive deployment periods. The first deployment period began on 12 February 2004 with the deployment during R/V *L'Atalante* cruise PIRATA FR-12 at 0°0.2′N, 23°6.8′W. On 29 May 2005, during R/V *Le Suroit* cruise PIRATA FR-13, the mooring was recovered and during the same day redeployed at 0°0.0′N, 23°7.5′W. This mooring was then recovered on 19 June 2006, during R/V *Meteor* cruise 68/2. During both deployment periods the mooring was equipped with two ADCPs, an upward looking 300-kHz Workhorse ADCP with 4 m vertical resolution, and a downward looking 75-kHz Long Ranger ADCP with 16 m vertical resolution (Table 1; see *Brandt et al.* [2006] for an analysis of velocity data from the first deployment period). The upward looking Workhorse ADCPs during both periods covered the whole distance between instrument depth and sea surface and the downward looking Long Ranger ADCPs had a measurement range of about 600 m. Sidelobe receptions of the upward looking ADCPs led to a degradation of data quality near the surface and approximately the upper 10% of measurement range were lost owing to sidelobe surface reflections. Technical details like transducer depth, bin length, center depth of first bin, as well as range and standard deviation of mooring excursions are summarized in Table 1. ADCP data of both instruments from each individual equatorial mooring at 35°W and 23°W have been combined to a continuous data set. The combined data sets have variable depth limits due to mooring motions and in each case have a gap of about 30 m arising from the separation of the two ADCP transducers plus their individual blanking distance (see Table 1). These gaps were filled by a Lagrangian interpolation algorithm, and the accuracy of the interpolation was estimated as follows. Using the interpolated field as a reference, we introduced a similar gap, but with different temporal variability and repeated the interpolation. Statistics (reference versus interpolated field) showed a negligible mean difference (<1 cm s^{-1}) at a standard deviation of about 3–5 cm s^{-1}, which appears

Table 1. ADCP Parameters and Measurement Depths Including Vertical Mooring Movements for Upward and Downward Looking ADCPs at the Two Mooring Sites at 35°W, 0° and 23°W, 0° During Two Deployment Periods

Longitude	Upward/ Downward Looking ADCP	Deployment Period	Bin Length, m	Mean Transducer Depth, m	Mean Center Depth of Bin 1, m	SD of Center Depth of Bin 1,[a] m	Min. of Center Depth of Bin 1, m	Max. of Center Depth of Bin 1, m
35°W	up	1	8.7	148	135	4	129	159
35°W	down	1	17.4	153	175	4	169	199
23°W	up	1	4.0	103	97	7	85	131
23°W	down	1	16.0	113	138	7	125	173
23°W	up	2	4.0	88	82	14	42	129
23°W	down	2	16.0	100	124	14	86	171

[a]SD: standard deviation.

Table 2. Depth of Local Maxima of the Zonal Flow on the Equator at 35°W and 23°W, Together With Means, Standard Deviations, Standard Errors, and Numbers of Degrees of Freedom of Zonal Velocity Time Series[a]

	Depth, m	Mean, m s^{-1}	Standard Deviation, m s^{-1}	Standard Error, m s^{-1}	NDF
		Equator, 35°W			
Near surface	25	0.00	0.18	0.03	49
EUC	95	0.69	0.17	0.03	36
EIC, upper core	280	−0.05	0.09	0.03	10
Eastward core	345	0.02	0.08	0.02	16
EIC, lower core	455	−0.09	0.08	0.02	12
		Equator, 23°W			
Near surface	15	−0.15	0.21	0.02	101
EUC	85	0.72	0.15	0.02	55
EIC, upper core	250	−0.06	0.07	0.02	17
Eastward core	320	0.05	0.10	0.05	4
EIC, lower core	455	−0.12	0.05	0.01	23

[a]NDF, Numbers of Degrees of Freedom; EUC, Equatorial Undercurrent; EIC, Equatorial Intermediate Current.

small relative to the mean speed of the EUC (the gaps are near the EUC center). Finally the data (5 m resolution, 1 h intervals) are detided by applying a 40 h low-pass filter and by subsequent subsampling to 12 h resolution.

[11] Time-mean moored zonal velocities are calculated after subtracting annual and semiannual harmonics that are calculated from the moored time series. The standard errors of the moored mean currents were estimated by scaling the standard deviations with the numbers of degrees of freedom (NDF; see, e.g., Table 2) determined from the autocorrelation of the detided time series.

2.3. Isopycnic RAFOS Floats

[12] Acoustically tracked RAFOS floats [*Rossby et al.*, 1986] drifting along isopycnal surfaces were additionally used to study the equatorial circulation. For the calculation of float trajectories we used the arrival time data of acoustic signals stored by the floats. These signals were transmitted from seven different sound sources at a repetition period of 12 h. To get an optimum coverage the sound sources were distributed between 35°W and 10°W and between 10°S and 1°N. The RAFOS floats used here were equipped with a compressee adjusting the float compressibility to that of seawater [*Rossby et al.*, 1985]. They were ballasted to drift at the potential density surface $\sigma_\theta = 26.8$ kg m^{-3}. The floats were deployed along meridional sections at 35°W, 28°W, 23°W and 10°W during three different cruises: during R/V *Meteor* cruise 62/2 in August 2004, during R/V *Le Suroit* cruise PIRATA FR-13 in May 2005 and during R/V *Le Suroit* cruise EGEE 1 in June 2005. Owing to technical problems, only a few trajectories could be obtained. Here, we will only use trajectories from floats drifting in the equatorial band between 1°N and 1°S.

3. Zonal Flow in the Equatorial Atlantic

[13] The zonal velocity on the equator at 35°W and 23°W as measured by the moored ADCPs (Figure 2) shows the eastward flowing EUC as the dominant signal. The core depths (core velocities) in the Eulerian mean flow field are 95 m (69 ± 3 cm s^{-1}) at 35°W and 85 m (72 ± 2 cm s^{-1}) at 23°W, respectively. The seasonal cycle of the equatorial zonal velocity associated with the EUC shows a shallow current core during March to April and a deep current core during late summer to autumn. During the latter phase the ITCZ is farthest north, the zonal wind on the equator is westward, the zonal surface pressure gradient is strongest toward the east and the near-surface flow is strongest toward the west [*Provost et al.*, 2004; *Hormann and Brandt*, 2007]. In general, the EUC at 35°W extends deeper and has a larger vertical extent compared to the EUC at 23°W. The standard error of the mean zonal velocity in the depth range of the EUC is small, despite the large standard deviation of about 15 cm s^{-1}. This is due to the high NDF of the time series resulting from pronounced intraseasonal fluctuations (see Figure 2 and Table 2).

[14] Above the EUC the mean flow, as estimated by surface drifter trajectories, is westward [*Lumpkin and Garzoli*, 2005]. Their climatology, yielding a zonal flow on the equator of −13 ± 15 cm s^{-1} at 35°W and −19 ± 14 cm s^{-1} at 23°W, can be compared to the uppermost ADCP measurements. The upward looking ADCP at 23°W yielded better data to shallower depths than did the instrument at 35°W owing to a shallower instrument position and less range reduction associated with surface reflections (Table 1). The moored mean near-surface velocity of 0 ± 3 cm s^{-1} in 25 m depth at 35°W and −15 ± 2 cm s^{-1} in 15 m depth at 23°W are smaller than the drifter velocities from the climatology. This discrepancy may result from the vertical shear present in the upper 20 m of the water column that was not covered by moored observations and is completely missed by standard shipboard observations.

[15] Below the EUC the zonal flow measured by the moored ADCPs is mostly westward and associated with the EIC (Figure 2). The deeper current meters at 35°W, down to 1100 m, also recorded predominantly westward velocities (Figure 3), which confirm previous results obtained from shipboard measurements at 35°W showing westward velocities in the depth range from below the EUC down to 2500 m [*Schott et al.*, 2003]. The amplitudes of the annual harmonics of the deeper velocity time series are larger than 10 cm s^{-1} at 500 m, 652 m, and 809 m with maximum eastward velocities in July, May, and March, respectively. These findings are in general agreement with the presence of downward propagating Rossby beams as already suggested from the analysis of meridional ship sections taken along 35°W by *Brandt and Eden* [2005].

[16] *Ollitrault et al.* [2006], analyzing trajectories of acoustically tracked floats drifting at 750 to 850 m also obtained a mean westward velocity on the equator of −6 ± 2 cm s^{-1} between 33°W and 20°W that was attributed to the EIC. The moored mean at 35°W at about 800 m depth yields −8 ± 4 cm s^{-1} (Figure 3), slightly larger than the float velocity, but in agreement within the standard errors of both observations.

[17] The mean flow structure obtained in the western and central Atlantic shows many similarities with that of the Pacific. *Firing et al.* [1998] described a westward EIC in the depth range 250–500 m using direct current measurements from 41 sections taken along 159°E within about 16 months. Below 500 m, down to 2500 m the flow was still mostly westward, however, superimposed by current

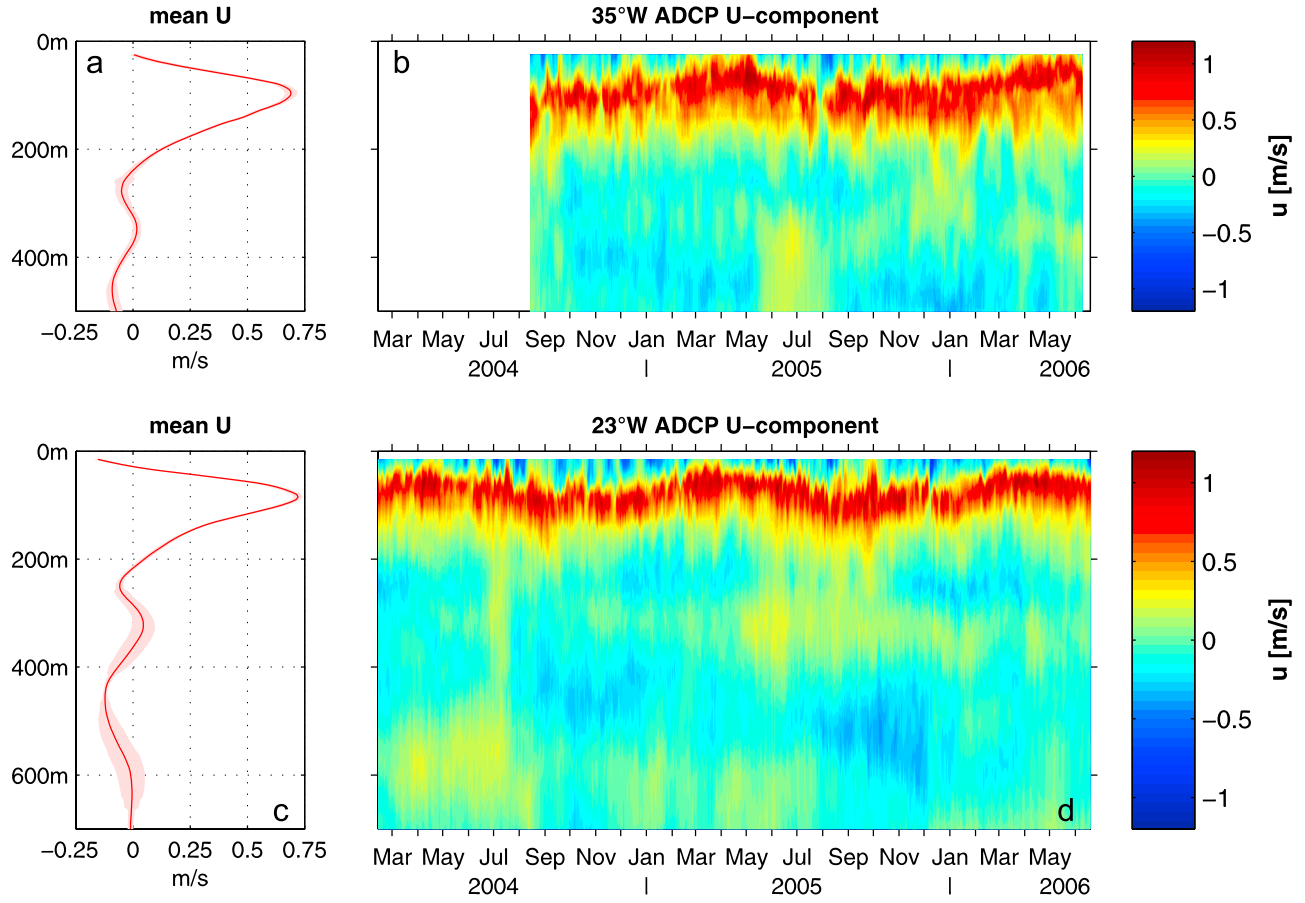

Figure 2. (a, b) Zonal velocity at the equator, 35°W from two 150-kHz narrowband acoustic Doppler current profilers (ADCPs), and (c, d) zonal velocity at the equator, 23°W from 300-kHz Workhorse ADCPs and 75-kHz Long Ranger ADCPs. Data are detided, and data gaps in between the instruments were interpolated. The mean flow is calculated by subtracting the annual and semiannual harmonics (Figures 2a and 2c, solid red line) with standard error (shaded).

bands with short vertical scales. Using direct current measurements of the upper 400 m, *Johnson et al.* [2002] found a westward strengthening the EIC with strong westward velocities at about 350 m depth in the western Pacific west of 155°W and weak or slightly eastward flow east of that longitude at the same depth.

[18] In our moored records from 35°W and 23°W, two cores of westward flow can be identified in the EIC depth range. The upper core of the EIC deepens from about 250 m at 23°W to about 280 m at 35°W, following the depth changes of the lower EUC limit located above. In contrast, the lower core of the EIC stays at the same depth from 23°W to 35°W (Figure 2 and Table 2). Between the two westward flowing cores insignificant mean eastward flow is found (Figure 2 and Table 2). The particularly large standard error at 23°W below the EUC is predominantly due to strong interannual variability that will be discussed in the following.

4. Oxygen Tongues and Zonal Jets

[19] The oxygen distribution in the ocean is a result of a subtle balance between supply via advection and diffusion and oxygen consumption as a result of heterotrophic respiration. In the tropical Atlantic, oxygen minimum zones are located north and south of the equator in the shadow zones of the ventilated thermocline [*Luyten et al.*, 1983]. The 23°W section from 4°S to 15°N that was taken during June–July 2006 cuts through the oxygen minimum zone of the tropical North Atlantic as well as through the equatorial belt (Figure 4). Minimum dissolved oxygen values of about 17 μmol kg^{-1} and 40 μmol kg^{-1} in the South and North Atlantic, respectively, are found at depths of 300 to 500 m or in the potential density range σ_θ = 26.6 kg m^{-3} to σ_θ = 27.1 kg m^{-3} [*Tsuchiya et al.*, 1992; *Karstensen et al.*, 2008; *Stramma et al.*, 2008]. The potential density surface σ_θ = 27.1 kg m^{-3} represents the boundary between Central Water and Antarctic Intermediate Water. In general, there is an eastward decrease of dissolved oxygen concentration throughout the central and intermediate water layers from the western boundary regime toward the sluggish flow near the eastern boundary. In the equatorial zone, westward and eastward subsurface jets are thus often characterized by low and high oxygen concentrations, respectively.

[20] Below the surface mixed layer, the EUC can be identified as an oxygen maximum. The cross-sectional area of the EUC with dissolved oxygen values larger than 130 μmol kg^{-1} as well as the oxygen maximum at about

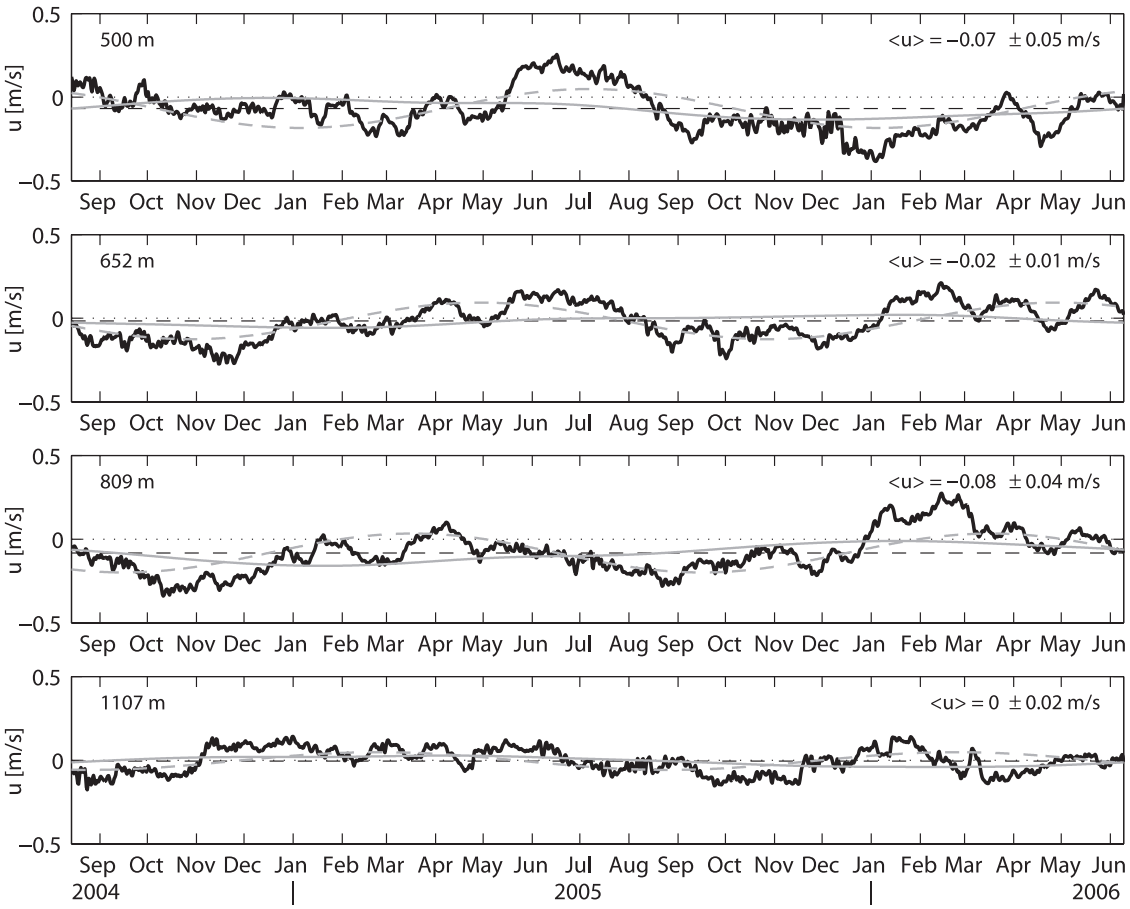

Figure 3. Zonal velocity time series from four Argonaut current meters at the equator, 35°W (solid black lines). Also given are interannual variations (solid gray lines) calculated by subtracting annual and semiannual harmonics and 9-month low-passed filtering, annual harmonics (dashed gray lines), and deployment-long means (black dashed lines) with standard error, calculated by subtracting annual and semiannual harmonics. Zero velocity is marked by dotted lines.

the core depth of the EUC decreases from 35°W to 10°W (Figure 5). The EUC mainly carries ventilated waters from the southern hemisphere supplied by the North Brazil Undercurrent in the potential density range of σ_θ = 24.5–26.8 kg m^{-3} [*Metcalf and Stalcup*, 1967; *Tsuchiya et al.*, 1992; *Schott et al.*, 1995, 2005]. The high-oxygen tongue associated with the EUC is flanked by low-oxygen waters transported westward with the northern and equatorial branches of the South Equatorial Current (nSEC and eSEC [*Stramma and Schott*, 1999]).

[21] Our shipboard observations during June–July 2006 show a secondary oxygen maximum underneath the EUC between the upper and lower cores of the EIC (Figure 5). This tongue of increased dissolved oxygen can be found at the three meridional sections along 35°W, 23°W and 10°W between about 300 and 350 m depth. It can also be followed along the equatorial section from 23°W to 10°W, with the maximum dissolved oxygen concentration decreasing from 130 μmol kg^{-1} at 23°W to 110 μmol kg^{-1} at 10°W (Figure 5d). As already discussed, the moored mean velocity profiles at 35°W and 23°W show an eastward velocity anomaly between two westward velocity cores associated with the EIC, which is associated with the oxygen tongue. Velocity measurements at 23°W during June–July 2006 strongly deviate from the annual mean profile for the period March 2005 to February 2006 suggesting that the high-oxygen tongue is generated by the eastward jet prevailing during the preceding year (Figure 6). Above and below this oxygen maximum, low oxygen values are associated with the upper and lower core of the westward flowing EIC. The dissolved oxygen concentration increases in these EIC cores from 10°W to 35°W.

[22] While the two EIC cores represent a drainage pathway for low-oxygen waters from the oxygen minimum zones, the eastward jet in between represents a pathway for high-oxygen waters toward the eastern equatorial Atlantic. Previous observational studies concentrated on the SICC and NICC which are located at about 2°S and 2°N and which are marked by high oxygen values originating in the North Brazil Undercurrent [*Tsuchiya et al.*, 1992; *Schott et al.*, 1995; *Boebel et al.*, 1999; *Bourlès et al.*, 2002]. In particular, the NICC was identified as an oxygen source for the oxygen minimum zone of the tropical North Atlantic [*Stramma et al.*, 2005]. In the observational data taken during June–July 2006, the highest oxygen values in the depth range of the tropical oxygen minimum zone are found directly at the equator (Figure 4).

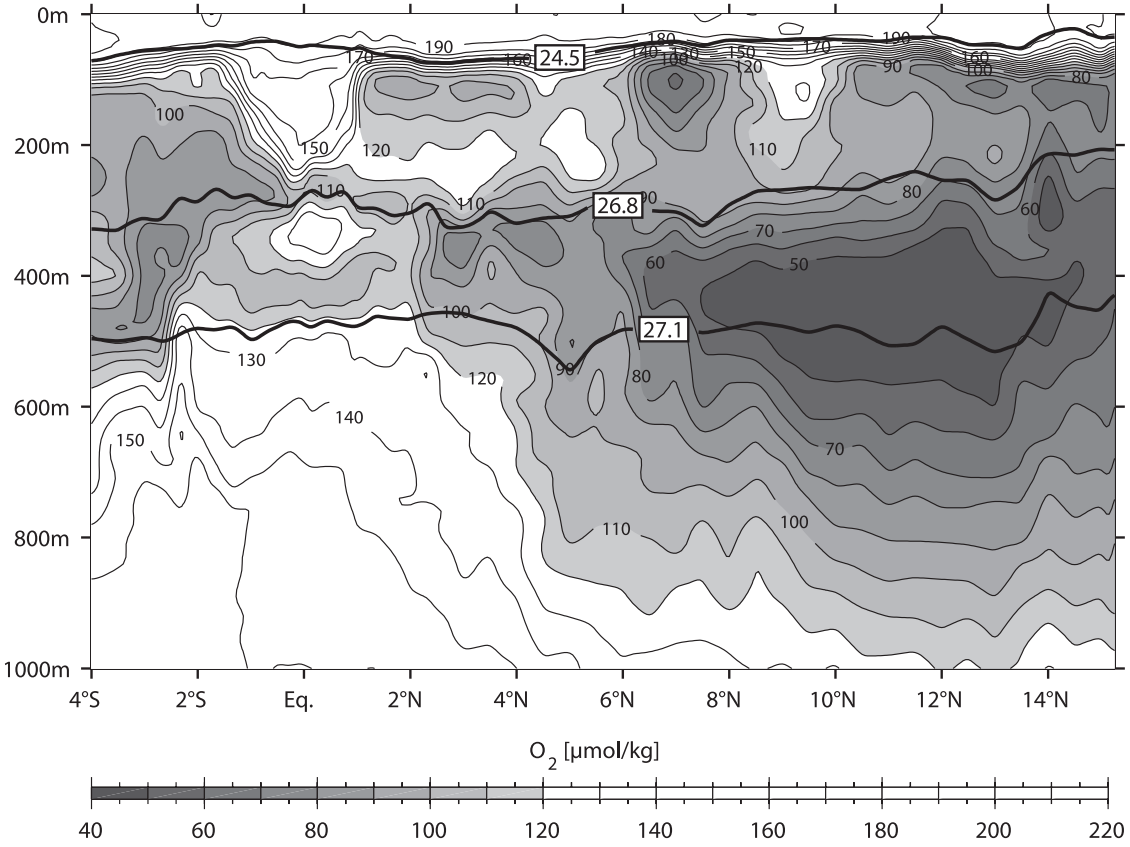

Figure 4. Dissolved oxygen (μmol kg^{-1}) along 23°W from shipboard observations in June–July 2006. Also included are depths of potential density surfaces (kg m^{-3}) (thick solid lines).

[23] The rapid exchange between the western boundary current regime and the eastern tropical Atlantic is captured by the RAFOS float trajectory shown in Figure 7. This float drifted on an isopycnal surface of $\sigma_\theta = 26.8$ kg m^{-3} at about 300 m depth. After a relative slow westward drift starting at 1°N, 28°10′W in August 2004 the float reached the equator at 35°W in December 2004 (Figure 8, yellow arrows). There the float stalled until April 2005. With the onset of eastward flow at 35°W (Figure 2), the float accelerated eastward and covered the distance between 35°W and 12°W in about 5 months, meandering around the equator along its way east. During the latter period, the Lagrangian zonal velocity fluctuated between 15 and 30 cm s^{-1} (Figure 8).

[24] Figure 8 summarizes direct velocity observations at the depth of the potential density surface $\sigma_\theta = 26.8$ kg m^{-3} from the two equatorial moorings at 35°W and 23°W and from RAFOS floats drifting near the equator between 1°S and 1°N. These observations suggest large zonal coherence of the eastward jet during May to September 2005.

[25] To address the relative importance of oxygen consumption, diapycnal turbulent diffusivity, and lateral eddy diffusivity, we applied the following Lagrangian diffusion equation for the oxygen decrease along the equator from 35°W to 10°W within the oxygen tongue at 300–350 m:

$$\frac{\partial C}{\partial t} = -JC + K_v \frac{\partial^2 C}{\partial z^2} + K_h \frac{\partial^2 C}{\partial y^2}. \qquad (1)$$

Here, C is the dissolved oxygen concentration, J is the dissolved oxygen consumption constant, K_v is the coefficient of the diapycnal turbulent diffusivity, and K_h is the coefficient of the lateral eddy diffusivity. The temporal derivative on the left-hand side of equation (1) must be balanced by the sum of the terms on the right-hand side. The temporal derivative can be estimated given the time that the RAFOS float (Figure 7) needed to travel from 35°W to 10°W, that is, about 6 months. The difference in the dissolved oxygen concentration at the core of the oxygen tongue from 35°W to 10°W measured in June–July 2006 was about -30 μmol kg^{-1}. Thus, the left-hand side of equation (1) is about -60 μmol kg^{-1} a^{-1}. The first term on the right-hand side of equation (1) describes the oxygen consumption, which we took from literature. *van Geen et al.* [2006] estimated the dissolved oxygen consumption constant by constraining a one-dimensional advection-diffusion model for the North Pacific oxygen minimum zone with Chlorofluorocarbon data. Using their best fit value of 0.041 a^{-1} and a mean dissolved oxygen concentration of 130 μmol kg^{-1}, we obtain an oxygen consumption rate of 5.3 μmol kg^{-1} a^{-1}. This is in general agreement with rates estimated for the Pacific and Atlantic oceans by *Karstensen et al.* [2008], who obtained a maximum oxygen consumption rate of about 10 μmol kg^{-1} a^{-1} below the euphotic zone decreasing exponentially with depth. The oxygen consumption is 1 order of magnitude smaller than the temporal derivative of equation (1) and cannot explain

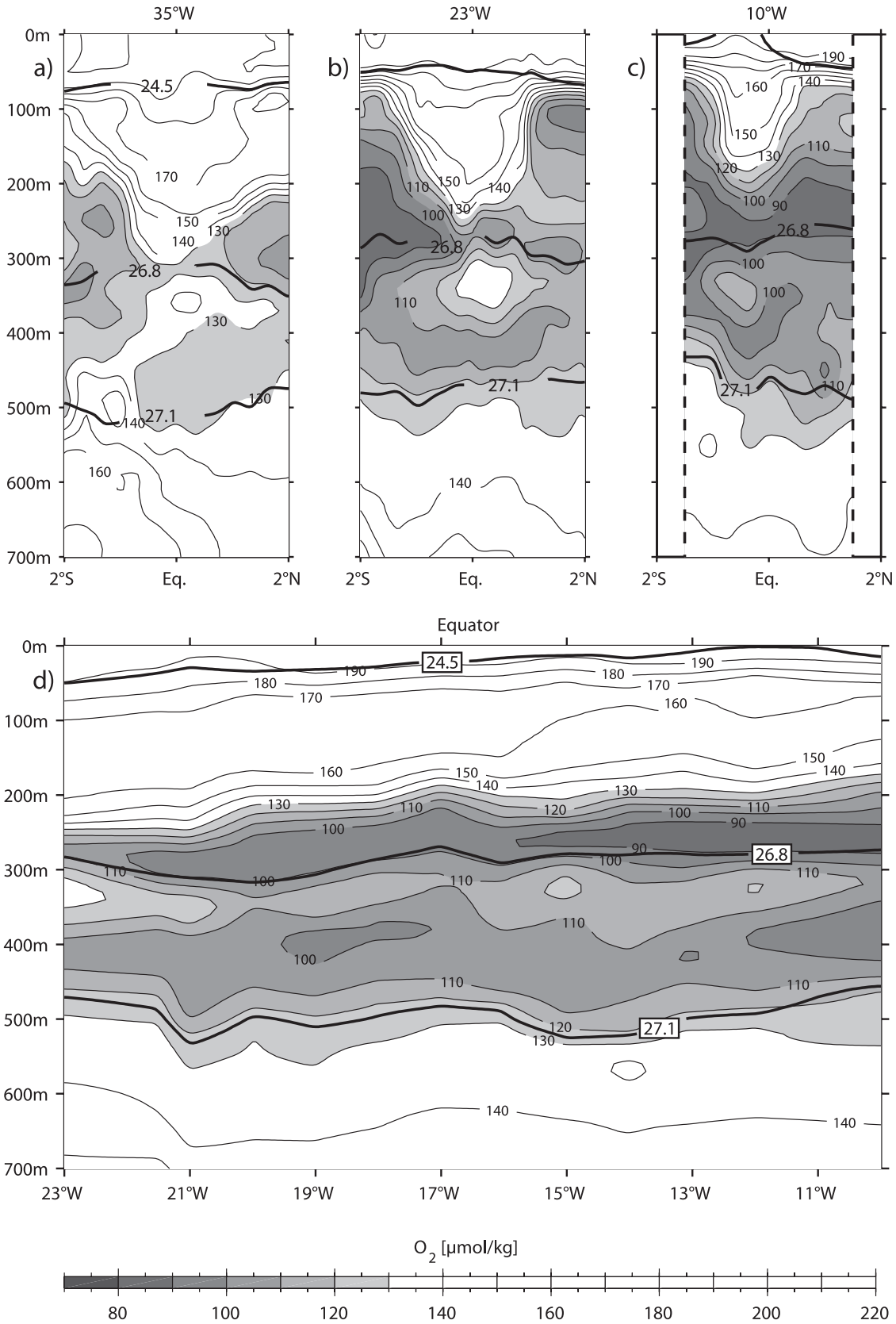
35°W
23°W
10°W
a)
b)
c)
d)
0m
100m
200m
300m
400m
500m
600m
700m
2°S
Eq.
2°N
Equator
23°W
21°W
19°W
17°W
15°W
13°W
11°W
24.5
26.8
27.1
O2 [µmol/kg]
80
100
120
140
160
180
200
220

Figure 5

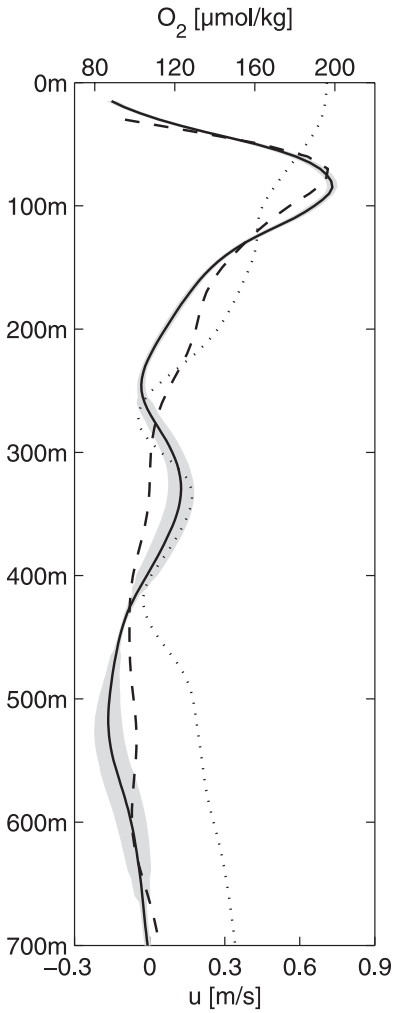

Figure 6. Zonal velocity (lower x axis) and dissolved oxygen (μmol kg^{-1}) (upper x axis) at 0°N, 23°W. Solid curve denotes zonal velocity obtained from moored instruments for the period March 2005 to February 2006 with standard error derived for the whole mooring period February 2004 to June 2006 (see Figure 2, shaded); dashed and dotted curves denote zonal velocity and dissolved oxygen, respectively, observed in June 2006 and averaged between 1°S and 1°N.

the decrease in oxygen concentration from west to east within the core of the oxygen tongue.

[26] The diapycnal turbulent diffusivity and the lateral eddy diffusivity are estimated by fitting second-order polynomials to vertical and horizontal profiles, respectively, through the oxygen maximum of the oxygen tongue. The obtained quadratic coefficients varied only slightly among the different oxygen distributions at 35°W, 23°W, and 10°W and correspond to a reduction in oxygen of 10 μmol kg^{-1} within mean distances of 37 m and 63 km above/below and north/south of the oxygen maximum, respectively. Using a diapycnal turbulent diffusivity coefficient of K_v = 10^{-5} m^2 s^{-1} that is at the upper bound of coefficients observed in the equatorial Pacific and Atlantic oceans below the EUC [*Gregg et al.*, 2003], a diapycnal turbulent diffusivity of -4.7 μmol kg^{-1} a^{-1} results. This value is of the same order of magnitude as the oxygen consumption, but it is also 1 order of magnitude smaller than the temporal derivative in equation (1).

[27] Using a lateral eddy diffusivity coefficient of K_h = 400 m^2 s^{-1} that can be considered as a typical value [*Eden et al.*, 2007], a lateral eddy diffusivity of -63 μmol kg^{-1} a^{-1} results. These rough estimates suggest that the reduction of the dissolved oxygen concentration from west to east in the core of the oxygen tongue is dominantly balanced by lateral eddy diffusivity. Substantial meridional velocity and oxygen fluctuations that possibly generate lateral eddy fluxes were in fact observed in June 2006 along the zonal section along 2°N in the depth range 400 to 600 m (Figure 9). Such fluctuations could result in an oxygen flux away from the equatorial region toward the oxygen minimum zones of the tropical North and South Atlantic.

5. Interannual Variability of Zonal Flow

[28] The zonal velocity on the equator at 23°W at about 300 m depth, shows predominantly westward flow from February 2004 to February 2005 and eastward flow during a 7-month period afterward (Figure 8) suggesting substantial interannual variability of the flow at intermediate depths. The strong year-to-year variability below the EUC at 23°W becomes also evident, when calculating successive annual mean zonal velocities, that is, from March 2004 to February 2005 and from March 2005 to February 2006, respectively (Figure 10). While the EUC remains almost unchanged, the annual mean velocities below 300 m differ by up to 20 cm s^{-1}. Main differences between the two annual mean profiles are a weakening of the upper core of the EIC, a strengthening of the eastward velocity anomaly between the two cores of the EIC associated with a lowering of the intermediate maximum, and a lowering of the lower core of the EIC. Strong interannual variability of the flow at intermediate depth was also found in a regional model of the tropical Atlantic forced by interannually varying wind fields [*Brandt and Eden*, 2005]. The simulated interannual variations in the velocity field were interpreted as downward propagating Kelvin and Rossby beams. However, these beams that are similar to those obtained for the annual cycle are composed of the first few baroclinic modes and

Figure 5. Dissolved oxygen (μmol kg^{-1}) from shipboard observations in June–July 2006 along meridional sections crossing the equator at (a) 35°W, (b) 23°W, and (c) 10°W, and (d) along the equator. Also included are depths of potential density surfaces (kg m^{-3}) (solid black lines). In the potential density range of σ_θ = 24.5–26.8 kg m^{-3} the EUC is supplied out of the North Brazil Undercurrent [e.g., *Schott et al.*, 2005]; the potential density surface σ_θ = 27.1 kg m^{-3} represents the boundary between the Central Water and the Antarctic Intermediate Water [*Karstensen et al.*, 2008]. Dashed lines in Figure 5c mark the measurement limits at 10°W.

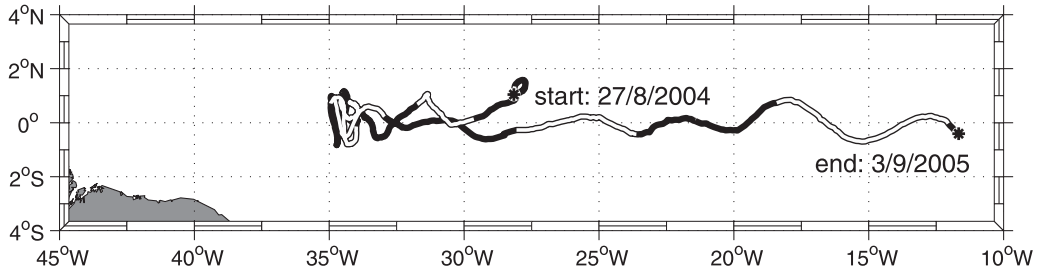

Figure 7. Trajectory of an acoustically tracked RAFOS float (RAFOS 623) drifting at potential density surface σ_θ = 26.8 kg m^{-3} (about 300 m depth). Even months are plotted white, and odd months are plotted black.

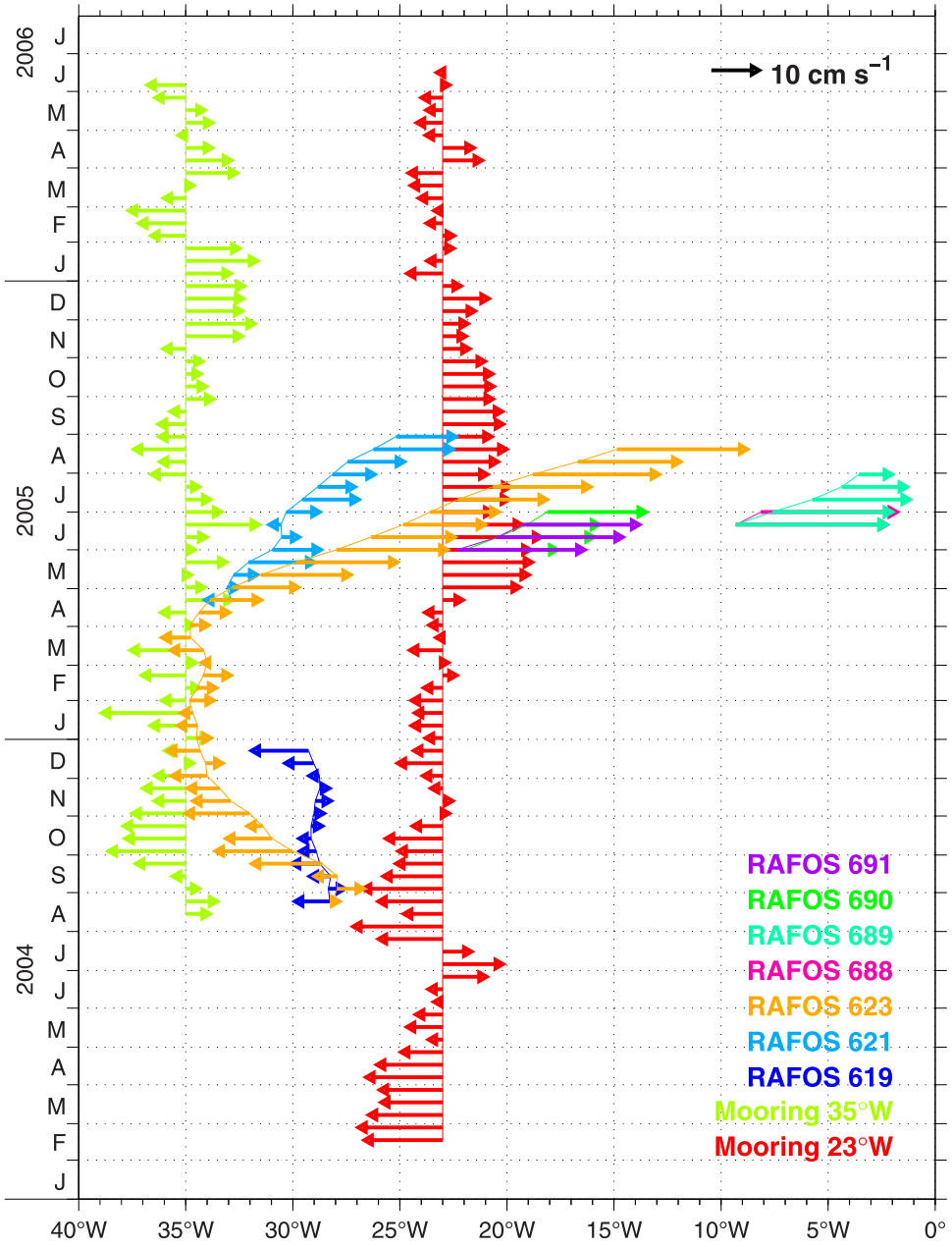

Figure 8. Zonal velocity at the equator at the depth of the potential density surface σ_θ = 26.8 kg m^{-3} (about 300 m depth) from moored observations at 35°W and 23°W as well as from RAFOS float trajectories drifting near the equator between 1°S and 1°N. Trajectory of RAFOS float 623 is shown in Figure 7.

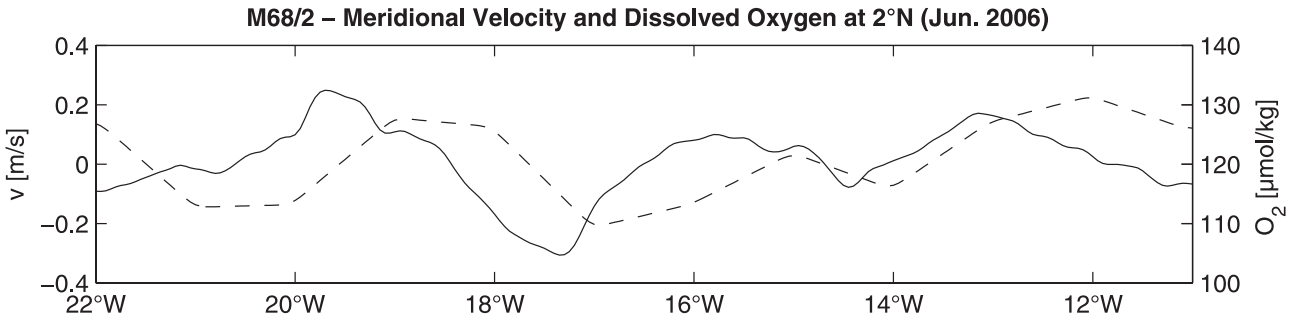

Figure 9. Meridional velocity component (solid, left axis) and dissolved oxygen (dashed, right axis) along 2°N averaged between 400 and 600 m depth from shipboard observations in June 2006.

are not able to explain the short vertical scales associated with the observed eastward jet within the EIC.

[29] Top to bottom velocity profiles have revealed the existence of high baroclinic mode variability in the equatorial Atlantic, occupying almost the whole water column below the EUC [*Ponte et al.*, 1990; *Gouriou et al.*, 1999; *Schmid et al.*, 2005; *d'Orgeville et al.*, 2007]. These stacked jets are characterized by alternating zonal flow with amplitudes of up to 20 cm s^{-1} and a meridional scale of about 1° in latitude. In the deeper ocean, their vertical wavelengths peak at about 600 m, which corresponds to vertical modes 14 through 16 [*Gouriou et al.*, 1999; *Eden and Dengler*, 2008]. Here, we have performed a vertical mode decomposition of a top to bottom mean density profile from the central equatorial Atlantic. The resulting dimensionless vertical structure functions were then fitted to the vertically detrended 23°W mooring data between 200 m and 700 m using a covariance criterion. The obtained vertical mode spectrum (Figure 11a) shows higher energy levels at vertical modes 12 through 20, with a distinct peak at mode 15. A comparison between this vertical mode spectrum and a vertical mode spectrum calculated from velocity data between 700 and 2000 m is depicted in Figure 11a. The used 47 deep zonal velocity profiles are acquired between 0.5°S and 0.5°N and between 35°W and 23°W. The mean deep vertical mode spectrum shows smaller energy levels than the shallow vertical mode spectrum, while single deep vertical mode spectra may overcome the energy levels of the mean shallow vertical mode spectrum. However, largest energy levels in the deep spectrum are found between mode 13 and 21 suggesting that the high baroclinic mode fluctuations at shallower depth have similar vertical wavelengths as the stacked jets in the deeper water column as analyzed by *Eden and Dengler* [2008].

[30] A description of the temporal variability of the stacked jets is particularly difficult owing to their long timescales. While an analysis of extensive hydrographic data by *Johnson and Zhang* [2003] suggested a period of stacked jets of about 5 years, recent direct velocity observations show that individual jets seem to persist over a time span from 6 months to 2 years [*Send et al.*, 2002; *Schmid et al.*, 2005; *Bunge et al.*, 2006]. *Firing* [1988] described jet-like structures in the Pacific Ocean at intermediate depths below the EUC. In his observations, these jets were nearly constant in depth for about half of the 16-month time series, while constantly rising during the rest of the observational period. In our moored data set, the mode (mode 15, Figure 11b) that best represents the eastward jet has eastward velocities at 330 m from February 2005 to May 2006 (Figure 11c). The temporal behavior of the feature observed by us thus agrees with the temporal behavior of stacked jets observed previously.

[31] The high-resolution oxygen distribution of different meridional sections taken during R/V *Thalassa* cruise along 23°W in August 1999, during R/V *Ron Brown* cruise along 25°W in August 2003, and during R/V *Meteor* cruise

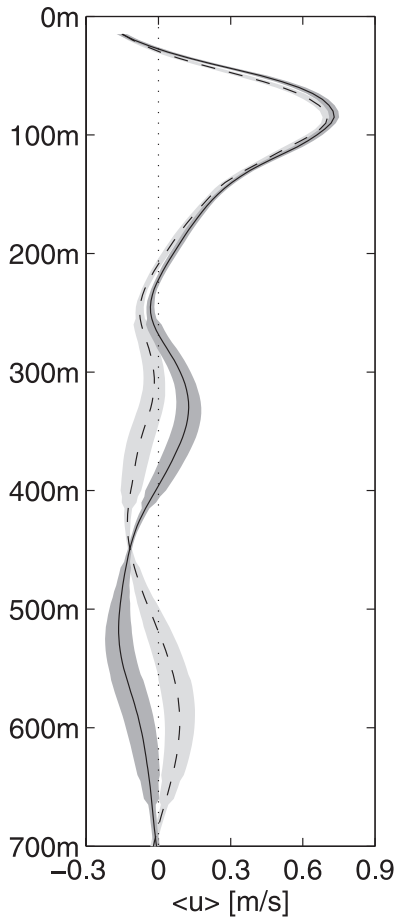

Figure 10. Annual mean equatorial zonal velocity profiles at 23°W for March 2004 to February 2005 (dashed) and March 2005 to February 2006 (solid). Standard errors are derived for the whole mooring period February 2004 to June 2006 (see Figure 2, shaded).

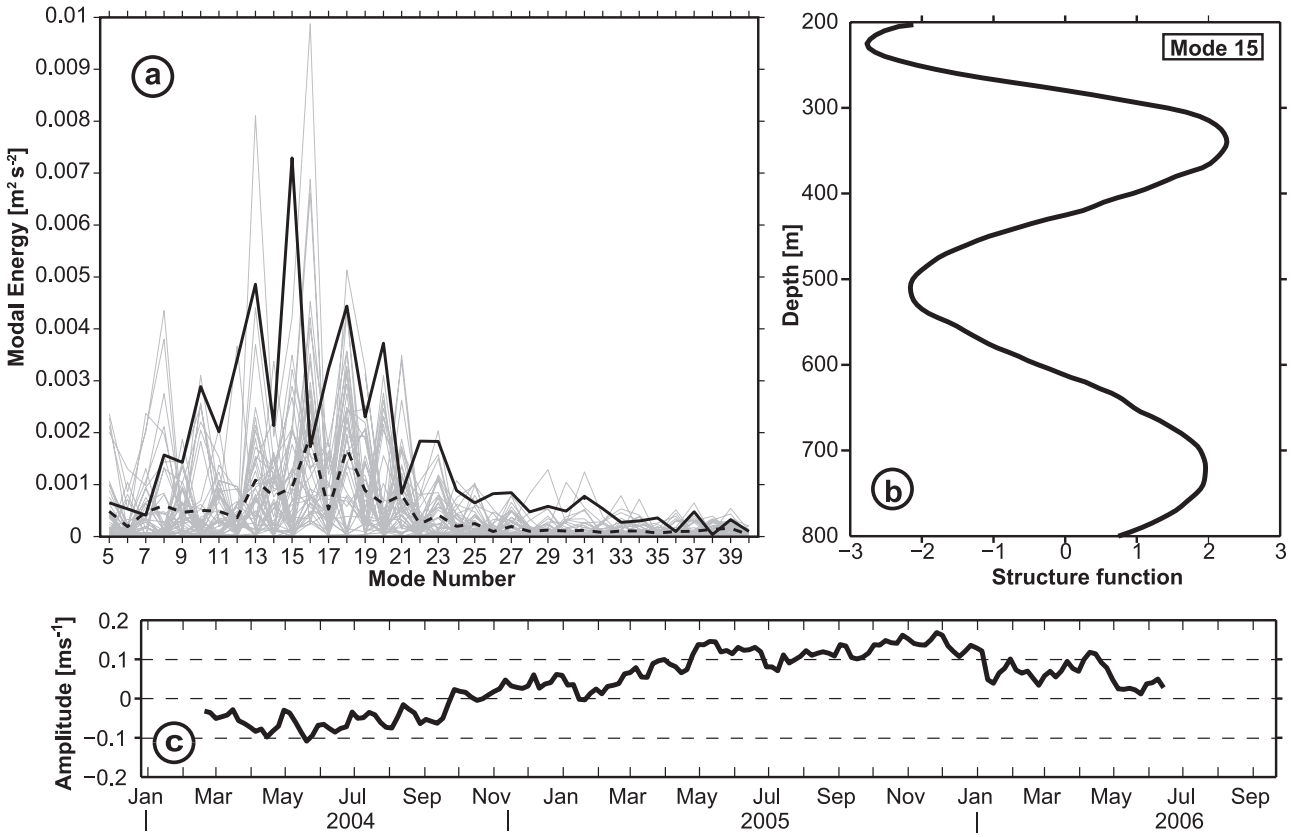

Figure 11. (a–c) Vertical mode analysis of zonal velocity at the equator at 23°W. Vertical mode spectrum (Figure 11a) was obtained by fitting dimensionless vertical structure functions to moored velocity data from below the EUC between 200 and 700 m (thick solid line) using a covariance criterion. In Figure 11b the dimensionless vertical structure function of mode 15 is shown, and in Figure 11c the time series of the corresponding amplitude is shown. Also included in Figure 11a are vertical mode spectra that are calculated from zonal velocity data between 700 and 2000 m (thin gray lines) of 47 deep velocity profiles measured between 0.5°S and 0.5°N and between 35°W and 23°W as well as their mean (dashed line).

along 23°W in June–July 2006 (Figure 12) additionally suggest a large variability in the occurrence of the jets in the central equatorial Atlantic. During August 1999 and August 2003 the dissolved oxygen concentration at intermediate depth (300 to 700 m) does not show an equatorial oxygen maximum. During August 2003 the oxygen concentration is enhanced away from the equator, particularly at about 1.5°N. This structure can be explained by the presence of the SICC and NICC with eastward core velocities larger than 10 cm s^{-1} as found in the mean zonal velocity field obtained from 11 different ship sections in the central equatorial Atlantic [*Brandt et al.*, 2006]. However, during June–July 2006 the situation changed and maximum dissolved oxygen concentration was found right on the equator at 300 m to 350 m depth that could be explained by the presence of a strong eastward zonal jet prevailing during the preceding year.

6. Summary and Discussion

[32] The availability of about 22-month- and 28-month-long velocity time series from 35°W and 23°W allows for the first time to determine annual mean zonal velocities at two separate equatorial positions unbiased by seasonal Rossby waves. It was shown that during the observational period a westward flowing EIC was present at 35°W and 23°W consisting of two current cores at about 250 m and 450 m depth, respectively. The upper core deepens westward from 23°W (mean velocity of 6 ± 2 cm s^{-1}) to 35°W (mean velocity of 5 ± 3 cm s^{-1}) by about 30 m. The lower core is about twice as strong with 12 ± 1 cm s^{-1} at 23°W and 9 ± 2 cm s^{-1} at 35°W.

[33] A similar two-core structure of the EIC was simulated in a high-resolution model of the Atlantic Ocean [*Böning and Kröger*, 2005]. However, the simulated mean core velocities were substantially smaller than observed. Other models likewise show weak time-mean currents at intermediate depths [*Jochum and Malanotte-Rizzoli*, 2003; *Brandt and Eden*, 2005; *Eden*, 2006]. In general, the recent model developments have shown that the time-mean current structure and strength improves when switching from low to high resolution [*Hüttl and Böning*, 2006, Figure 3], suggesting that a further reduction of vertical and/or lateral mixing of momentum may improve the simulation of the mean equatorial flow field at intermediate depths.

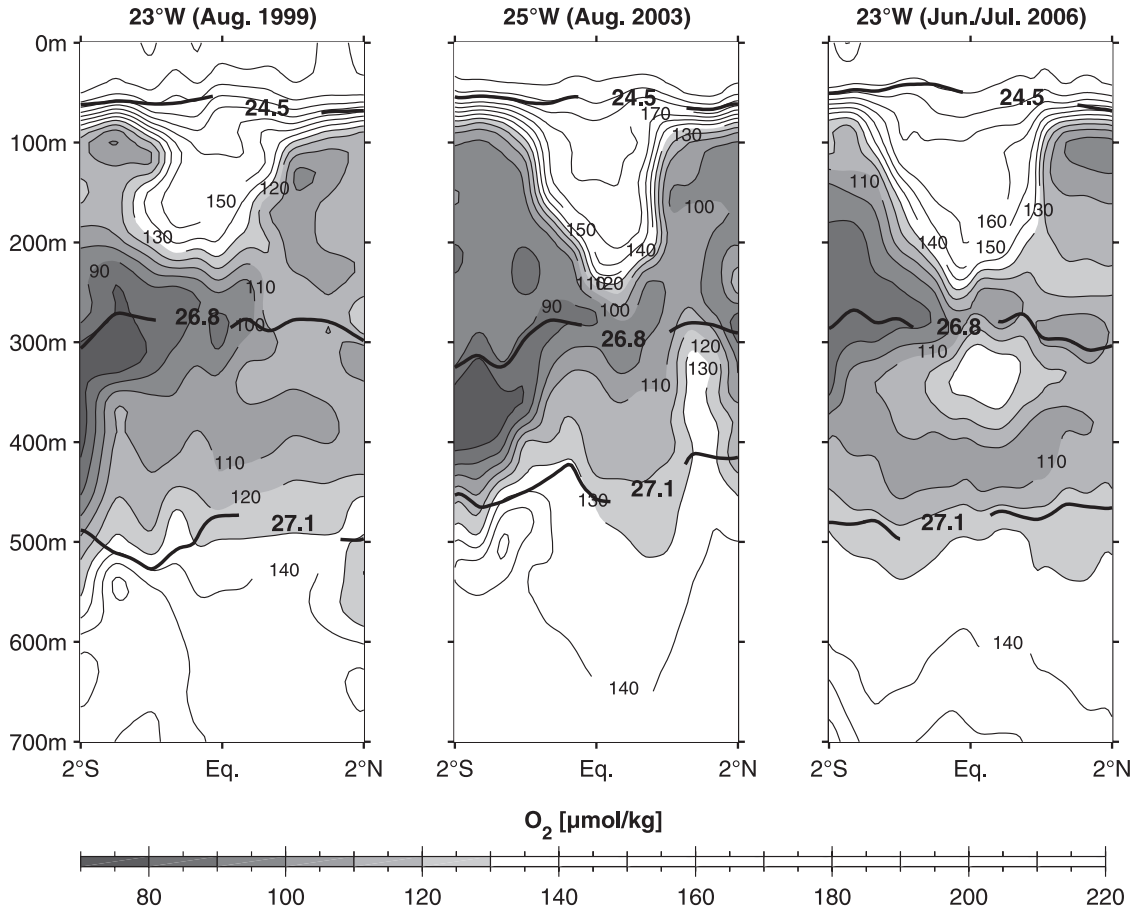

Figure 12. Dissolved oxygen (μmol kg^{-1}) from shipboard observations along meridional sections crossing the equator at 23°W in August 1999, at 25°W in August 2003, and at 23°W in June–July 2006. Also included are depths of potential density surfaces (kg m^{-3}) (solid black lines).

[34] Between the two westward flowing EIC cores, a weak mean eastward flow was present during the mooring period. At 23°W, the eastward flow was particularly strong from May to September 2005 in the depth range between 300 and 350 m while during the same period 1 year earlier the flow was westward or only slightly eastward (Figure 8). This strong year-to-year variability below the EUC was emphasized by a comparison of two annual mean velocity profiles from 23°W (Figure 10). The eastward jet with an annual mean velocity of about 15 cm s^{-1} for the period March 2005 to February 2006 (Figure 8) was found to be responsible for the equatorial oxygen maximum in the depth range 300–350 m observed during June–July 2006 (Figures 5 and 6). An analysis of the vertical scale suggested that the feature is best described by vertical mode number 15 that corresponds to a wavelength of about 600 m in the deep ocean. The temporal as well as vertical scale both agree with characteristics of stacked jets in the deep Atlantic Ocean as previously observed.

[35] The large timescale associated with the stacked jets results in small NDF and correspondingly in large standard errors of the mean zonal velocity profiles below the EUC (Figure 2). While the interannual variations may exceed 20 cm s^{-1} in the depth range 200 to 500 m, the deeper velocity observations at 35°W show strong interannual fluctuations, as well, with observed interannual fluctuations at 800 m reaching 7 cm s^{-1} (Figure 3). To estimate the effect of the stacked jets on the mean zonal velocity, we compare the moored means at 35°W and 23°W with mean zonal velocities calculated from shipboard velocity data taken at 35°W (Figure 13a) and between 23°W and 28.5°W (Figure 13b), respectively. The shipboard observations span a period from 1990 to 2006 [cf. *Schott et al.*, 2003; *Brandt et al.*, 2006; *Hormann and Brandt*, 2007]. The amplitude of the high-baroclinic mode variability in the shipboard means is smaller compared to the moored means. Particularly at 35°W, where a large number of shipboard observations is available, there is an almost depth-independent westward flow below 500 m suggesting the presence of a mean EIC independent on the existence of stacked jets.

[36] Eastward jets as the one observed from May to September 2005 at 300 to 350 m contribute to the ventilation of the eastern equatorial Atlantic: the fast exchange between western boundary current regime and the eastern equatorial Atlantic could be demonstrated by an isopycnic RAFOS float drifting within a few months along the equator from 35°W to 12°W (Figure 7). By applying a simple advection-diffusion balance it is suggested that the oxygen decrease from 35°W to 10°W within the observed oxygen tongue is mainly balanced by lateral eddy diffusivity, oxygen consumption and diapycnal turbulent diffusivity playing only a minor role. As observed velocities in the

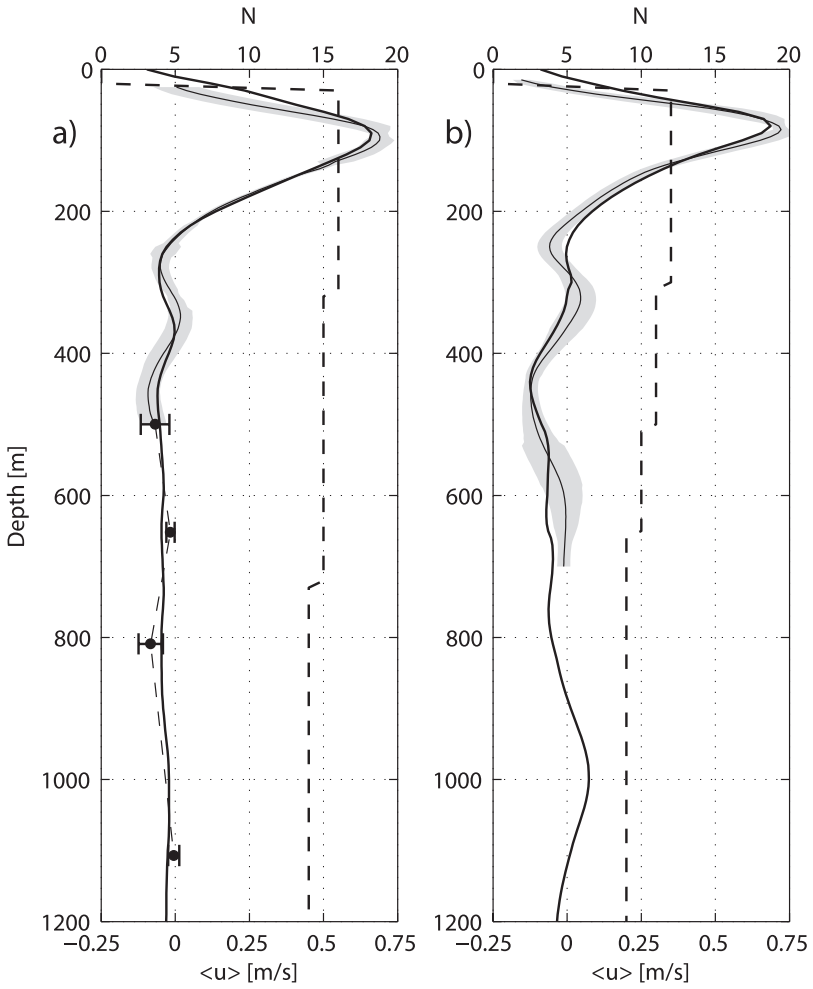

Figure 13. Mean equatorial zonal velocity profiles at (a) 35°W and (b) about 23°W, from shipboard observations (thick solid line), moored ADCP observations (thin solid line) with standard error (see Figure 2, shaded), and moored Argonaut observations (thin dashed line, black circles with error bars). The number of available shipboard observations from different ship sections at 35°W (Figure 13a) and between 23°W and 28.5°W (Figure 13b) is denoted by the thick dashed line (N, upper axis).

SICC and NICC are of similar magnitude as in the eastward jet described here, such balance may hold also for the off-equatorial countercurrents. The strong variability of the oxygen concentration in the region of the SICC and NICC during different years (Figure 12) consequently should result from interannual variations in the strength of the off-equatorial countercurrents.

[37] Our measurements along the 23°W section revealed that during June–July 2006 the equatorial oxygen maximum associated with the observed eastward jet was characterized by the highest oxygen concentrations in the isopycnal layer defined by potential density surfaces σ_θ = 26.8 kg m^{-3} and σ_θ = 27.1 kg m^{-3} from 4°S to 15°N (Figure 4). Besides the zonal supply pathways via the NECC system and the NICC, transporting high-oxygen waters from the western boundary eastward [*Stramma et al.*, 2005, 2008], equatorial zonal jets could significantly contribute, via lateral eddy fluxes, to the ventilation of the oxygen minimum zone of the tropical North Atlantic.

[38] **Acknowledgments.** This work was supported by the German Science Foundation (DFG) under contract SCHO 168/30-1, BR 2286/1-1, and FI 871/1-1 and by the Deutsche Bundesministerium für Bildung und Forschung (BMBF) as part of the Verbundvorhaben Nordatlantik under contract 03F0443B. We thank Carsten Eden for helpful discussions and Rainer Zantopp, Karina von Schuckmann, and Matthias Lankhorst for their help with the analysis and figures. The drifter climatology was developed by R. Lumpkin (NOAA/AOML) in collaboration with S. Garzoli and M. Pazos (NOAA/AOML), J. Redman (CIMAS), and Z. Garraffo (RSMAS, University of Miami). The NOAA R/V *Ronald Brown* 2003 cruise (chief scientists John Bullister and Nicolas Gruber) was completed under the NSF/NOAA-funded Repeat Hydrography Program, and data (ADCP P.I. Eric Firing and Julia M. Hummon and hydrography P.I. Gregory Johnson) were made available through the CLIVAR and Carbon Hydrographic Data Office, La Jolla, California.

References

Andrié, C., J. F. Ternon, M. J. Messias, L. Memery, B. Bourlès, Y. Gouriou, and C. Oudot (1998), Chlorofluoromethane distributions in the deep equatorial Atlantic during January–March 1993, *Deep Sea Res., Part I*, *45*, 903–930.

Boebel, O., R. E. Davis, M. Ollitrault, R. G. Peterson, P. L. Richardson, C. Schmid, and W. Zenk (1999), The intermediate depth circulation of the western South Atlantic, *Geophys. Res. Lett.*, *26*(21), 3329–3332.

Böning, C. W., and J. Kröger (2005), Seasonal variability of deep currents in the equatorial Atlantic: A model study, *Deep Sea Res., Part I*, *52*, 99–121.

Bourlès, B., M. d'Orgeville, G. Eldin, Y. Gouriou, R. Chuchla, Y. du Penhoat, and S. Arnault (2002), On the evolution of the thermocline

and subthermocline eastward currents in the Equatorial Atlantic, *Geophys. Res. Lett.*, *29*(16), 1785, doi:10.1029/2002GL015098.

Bourlès, B., et al. (2003), The deep currents in the eastern equatorial Atlantic Ocean, *Geophys. Res. Lett.*, *30*(5), 8002, doi:10.1029/2002GL015095.

Brandt, P., and C. Eden (2005), Annual cycle and interannual variability of the mid-depth tropical Atlantic Ocean, *Deep Sea Res., Part I*, *52*, 199–219.

Brandt, P., F. A. Schott, C. Provost, A. Kartavtseff, V. Hormann, B. Bourlès, and J. Fischer (2006), Circulation in the central equatorial Atlantic: Mean and intraseasonal to seasonal variability, *Geophys. Res. Lett.*, *33*, L07609, doi:10.1029/2005GL025498.

Bunge, L., C. Provost, J. Lilly, M. d'Orgeville, A. Kartavtseff, and J. L. Melice (2006), Variability of the horizontal velocity structure in the upper 1600 m of the water column on the equator at 10°W, *J. Phys. Oceanogr.*, *36*, 1287–1304.

d'Orgeville, M., B. L. Hua, and H. Sasaki (2007), Equatorial deep jets triggered by a large vertical scale variability within the western boundary layer, *J. Mar. Res.*, *65*, 1–25.

Eden, C. (2006), Mid-depth equatorial tracer tongues in a model of the Atlantic Ocean, *J. Geophys. Res.*, *111*, C12025, doi:10.1029/2006JC003565.

Eden, C., and M. Dengler (2008), Stacked jets in the deep equatorial Atlantic Ocean, *J. Geophys. Res.*, doi:10.1029/2007JC004298, in press.

Eden, C., R. J. Greatbatch, and J. Willebrand (2007), A diagnosis of thickness fluxes in an eddy-resolving model, *J. Phys. Oceanogr.*, *37*, 727–742.

Firing, E. (1988), Shallow equatorial jets, *J. Geophys. Res.*, *93*, 9213–9222.

Firing, E., S. E. Wijffels, and P. Hacker (1998), Equatorial subthermocline currents across the Pacific, *J. Geophys. Res.*, *103*, 21,413–21,423.

Fischer, J., P. Brandt, M. Dengler, M. Müller, and D. Symonds (2003), Surveying the upper ocean with the Ocean Surveyor: A new phased array Doppler current profiler, *J. Atmos. Oceanic Technol.*, *20*, 742–751.

Gouretski, V. V., and K. Jancke (1998), A new world ocean climatology: Objective analysis on neutral surfaces, *Tech. Rep. 3*, WHP Spec. Anal. Cent., Hamburg, Germany.

Gouriou, Y., B. Bourlès, H. Mercier, and R. Chuchla (1999), Deep jets in the equatorial Atlantic Ocean, *J. Geophys. Res.*, *104*, 21,216–21,226.

Gouriou, Y., et al. (2001), Deep circulation in the equatorial Atlantic Ocean, *Geophys. Res. Lett.*, *28*, 819–822.

Gregg, M. C., T. B. Sanford, and D. P. Winkel (2003), Reduced mixing from the breaking of internal waves in equatorial waters, *Nature*, *442*, 513–515.

Hazeleger, W., and P. de Vries (2003), Fate of the equatorial undercurrent in the Atlantic, in *Interhemispheric Water Exchange in the Atlantic Ocean*, edited by G. J. Goni and P. Malanotte-Rizzoli, *Elsevier Oceanogr. Ser.*, *68*, 175–191.

Hormann, V., and P. Brandt (2007), Atlantic Equatorial Undercurrent and associated cold tongue variability, *J. Geophys. Res.*, *112*, C06017, doi:10.1029/2006JC003931.

Hüttl, S., and C. W. Böning (2006), Mechanisms of decadal variability in the shallow subtropical-tropical circulation of the Atlantic Ocean: A model study, *J. Geophys. Res.*, *111*, C07011, doi:10.1029/2005JC003414.

Jochum, M., and P. Malanotte-Rizzoli (2003), The flow of AAIW along the equator, in *Interhemispheric Water Exchange in the Atlantic Ocean*, edited by G. J. Goni and P. Malanotte-Rizzoli, *Elsevier Oceanogr. Ser.*, *68*, 193–212.

Johnson, G. C., and D. Zhang (2003), Structure of the Atlantic Ocean equatorial deep jets, *J. Phys. Oceanogr.*, *33*, 600–609.

Johnson, G. C., B. M. Sloyan, W. S. Kessler, and K. E. McTaggert (2002), Direct measurements of upper ocean currents and water properties across the tropical Pacific during the 1990s, *Prog. Oceanogr.*, *52*, 31–61.

Karstensen, J., L. Stramma, and M. Visbeck (2008), Oxygen minimum zones in the eastern tropical Atlantic and Pacific oceans, *Prog. Oceanogr*, in press.

Liu, Z., S. G. H. Philander, and R. C. Pacanowski (1994), A GCM study of tropical-subtropical upper-ocean water exchange, *J. Phys. Oceanogr.*, *24*, 2606–2623.

Lumpkin, R., and S. L. Garzoli (2005), Near-surface circulation in the tropical Atlantic Ocean, *Deep Sea Res., Part I*, *52*, 495–518, doi:10.1016/j.dsr.2004.09.001.

Luyten, J. R., J. Pedlosky, and H. Stommel (1983), The ventilated thermocline, *J. Phys. Oceanogr.*, *13*, 292–309.

Malanotte-Rizzoli, P., K. Hedstrom, H. Arango, and D. B. Haidvogel (2000), Water mass pathways between the subtropical and tropical ocean in a climatological simulation of the North Atlantic Ocean circulation, *Dyn. Atmos. Oceans*, *32*, 331–371.

McCreary, J. P. (1984), Equatorial beams, *J. Mar. Res.*, *42*, 395–430.

McCreary, J. P., and P. Lu (1994), Interaction between the subtropical and equatorial ocean circulations: The subtropical cell, *J. Phys. Oceanogr.*, *24*, 466–497.

Metcalf, W. G., and M. C. Stalcup (1967), Origin of the Atlantic Equatorial Undercurrent, *J. Geophys. Res.*, *72*, 4959–4974.

Ollitrault, M., M. Lankhorst, D. Fratantoni, P. Richardson, and W. Zenk (2006), Zonal intermediate currents in the equatorial Atlantic Ocean, *Geophys. Res. Lett.*, *33*, L05605, doi:10.1029/2005GL025368.

Ponte, R., J. Luyten, and P. L. Richardson (1990), Equatorial deep jets in the Atlantic Ocean, *Deep Sea Res.*, *37*, 711–713.

Provost, C., S. Arnault, N. Chouaib, A. Kartavtseff, L. Bunge, and E. Sultan (2004), TOPEX/Poseidon and Jason equatorial sea surface slope anomaly in the Atlantic in 2002: Comparison with wind and current measurements at 23W, *Mar. Geod.*, *27*, 31–45.

Rossby, T., E. R. Levine, and D. N. Conners (1985), The isopycnal Swallow float: A simple device for tracking water parcels in the ocean, *Prog. Oceanogr.*, *14*, 511–525.

Rossby, T., D. Dorson, and J. Fontaine (1986), The RAFOS system, *J. Atmos. Oceanic Technol.*, *3*(4), 672–679.

Schmid, C., B. Bourlès, and Y. Gouriou (2005), Impact of the deep equatorial jets on the zonal transport in the Atlantic, *Deep Sea Res., Part II*, *52*, 409–428.

Schott, F. A., L. Stramma, and J. Fischer (1995), The warm water inflow into the western tropical Atlantic boundary regime, spring 1994, *J. Geophys. Res.*, *100*, 24,745–24,760.

Schott, F. A., M. Dengler, P. Brandt, K. Affler, J. Fischer, B. Bourlès, Y. Gouriou, R. L. Molinari, and M. Rhein (2003), The zonal currents and transports at 35°W in the tropical Atlantic, *Geophys. Res. Lett.*, *30*(7), 1349, doi:10.1029/2002GL016849.

Schott, F. A., J. P. McCreary, and G. C. Johnson (2004), Shallow overturning circulations of the tropical-subtropical oceans, in *Earth*'s *Climate: The Ocean-Atmosphere Interaction and Climate Variability*, *Geophys. Monogr. Ser.*, vol. 147, edited by C. Wang, S.-P. Xie, and J. A. Carton, AGU, Washington, D. C.

Schott, F., M. Dengler, R. J. Zantopp, L. Stramma, J. Fischer, and P. Brandt (2005), The shallow and deep western boundary circulation of the South Atlantic at 5°–11°S, *J. Phys. Oceanogr.*, *35*, 2031–2053.

Send, U., C. Eden, and F. Schott (2002), Atlantic equatorial deep jets: Space-time structure and cross-equatorial fluxes, *J. Phys. Oceanogr.*, *32*, 891–902.

Stramma, L., and F. Schott (1999), The mean flow field of the tropical Atlantic Ocean, *Deep Sea Res., Part II*, *46*, 279–303.

Stramma, L., S. Hüttl, and J. Schafstall (2005), Water masses and currents in the upper tropical Northeast Atlantic off northwest Africa, *J. Geophys. Res.*, *110*, C12006, doi:10.1029/2005JC002939.

Stramma, L., P. Brandt, J. Schafstall, F. Schott, J. Fischer, and A. Körtzinger (2008), The oxygen minimum zone in the North Atlantic south and east of the Cape Verde Islands, *J. Geophys. Res.*, doi:10.1029/2007JC004369, in press.

Thierry, V., A. M. Treguier, and H. Mercier (2004), Numerical study of the annual and semi-annual fluctuations in the deep equatorial Atlantic Ocean, *Ocean Modell.*, *6*, 1–30.

Tsuchiya, M., L. D. Talley, and M. S. McCartney (1992), An eastern Atlantic section from Iceland southward across the equator, *Deep Sea Res., Part A*, *39*, 1885–1917.

van Geen, A., W. M. Smethie Jr., A. Horneman, and H. Lee (2006), Sensitivity of the North Pacific oxygen minimum zone to changes in ocean circulation: A simple model calibrated by chlorofluorocarbons, *J. Geophys. Res.*, *111*, C10004, doi:10.1029/2005JC003192.

B. Bourlès, Centre IRD de Brest, 29280 Plouzané, France.

P. Brandt, M. Dengler, J. Fischer, V. Hormann, F. A. Schott, and L. Stramma, IFM-GEOMAR, Leibniz-Institut für Meereswissenschaften, D-24105 Kiel, Germany. (pbrandt@ifm-geomar.de)